An Optimal Wheel Torque Distribution Controller for Automated Vehicle Trajectory Following

Ling-Yuan Hsu and Tsung-Lin Chen

***Abstract*—This paper proposes an automated vehicle trajectory following system that uses four constrained wheel torques to regulate a vehicle on a reference trajectory. The constrained wheel torques can be achieved using the two-wheel drive and differential brakes. The proposed control algorithm is developed using the following steps. First, the sliding-mode control is used to find stability constraints for trajectory following when the vehicle system is subjected to modeling errors. Second, these stability constraints, along with other actuator constraints, are particularly tuned for the proposed control distribution method. The proposed control distribution method determines four longitudinal tire forces and minimizes actuator control efforts. Finally, these tire forces are converted to traction/braking wheel torques. The proposed method has the following advantages: 1) It achieves both robust trajectory following and optimal control efforts, 2) the optimal control effort is obtained analytically instead of from a numerical search, and 3) the robust performance of this vehicle control system can be theoretically verified. The proposed method is evaluated using numerical simulations on two front-drive vehicle models: a full-state vehicle model and a sedan model from the Carsim commercial software. The simulation results indicate that, in both cases, the proposed method can regulate the vehicle to finish a "double-lane change" when the vehicle is moving at an initial speed of 90 km/h. The maximum lateral acceleration is 6.56 m/s^2, and the regulated position error is less than 6.9 cm.**

***Index Terms*—Automated vehicle trajectory following, control distribution, differential torque controls, Karush–Kuhn–Tucker (KKT) theorem, optimization, sliding-mode controls, vehicle control systems.**

I. Introduction

In RECENT years, several studies have used the direct yaw moment control (DYC) for lane following, which is to generate controlled yaw moments on a vehicle to regulate vehicle trajectories [1]–[4]. In most cases, this controlled yaw moment is generated by the steering wheel control because it is simple and straightforward [2], [5], [6]. A number of studies have proposed the use of the differential torque (brake) system to generate this yaw moment [3], [4], [7]. Although the use of the differential torque (brake) approach is complex, it has several advantages, such as no additional mechanical or hydraulic components are required, and the steering system can remain intact for other control applications. Both approaches have been proven to be effective. Currently, several differential torque approaches only determine a lumped traction/braking torque on tires either at two sides (left and right) or one side, instead of for four tires independently. This substantially reduces the complexity of control algorithms. However, from the control viewpoint, these simplified control approaches may limit the effectiveness of vehicle control.

Most DYC systems are developed using a hierarchical architecture to reduce the complexity of the controller design [2], [4], [7], [8]. When using this hierarchical architecture for the differential torque system, the control algorithm first determines the virtual tire forces and/or moments for regulating vehicle trajectory. Subsequently, this virtual entity is distributed to four tire forces using control distribution [2], [4], [7]–[9]. Finally, these distributed tire forces are transformed into traction/braking wheel torques. Therefore, this approach involves two research topics: robust feedback control and control distribution. For feedback control, system stability must be examined for the overall system instead of for each hierarchical layer; otherwise, the transient response of each layer may endanger the stability of the overall system [8]. For example, dynamics occur between tire forces and traction/braking torques. These dynamics are often neglected when calculating the applied wheel torques from the designated tire forces, which may result in stability problems when working toward the better performance of the vehicle.

For control distribution, Ono *et al.* [10] propose a vehicle control system using four wheel steering angles and four wheel traction/braking torques. The control algorithm is developed using a hierarchical architecture, and the control inputs are distributed using a nonlinear optimization process that maximizes the grip margin for each tire. The optimal solution to this distribution problem is obtained using a recursive method. This study focuses on the control distribution. Therefore, the stability analysis of this hierarchical control architecture is omitted. Tjønnås and Johansen [8] propose a vehicle control system similar to that in [10]. The difference is that the control distribution method determines control inputs by minimizing the steering angle and slip ratios. The system stability is theoretically verified for the case of limited model errors. Andreasson and Bünte [11] propose a generic vehicle control method, in which the control inputs are four wheel steering angles, four wheel torques, and four tire loads. The proposed control distribution is achieved by adding more constraints to this distribution problem (underdetermined) and yielding an overdetermined problem that can be solved using the least squares method. A possible disadvantage is that the stability constraint may not be completely fulfilled because of the nature of an overdetermined

Manuscript received February 8, 2012; revised June 18, 2012 and December 14, 2012; accepted January 17, 2013. Date of publication February 12, 2013; date of current version July 10, 2013. The review of this paper was coordinated by Dr. S. Anwar.

The authors are with the Department of Mechanical Engineering, National Chiao Tung University, Hsinchu 30010, Taiwan (e-mail: lance1214@gmail.com; tsunglin@mail.nctu.edu.tw).

Color versions of one or more of the figures in this paper are available online at http://ieeexplore.ieee.org.

Digital Object Identifier 10.1109/TVT.2013.2246593

problem. In summary, two major issues are encountered in control distribution. First, the stability of the feedback system may not be guaranteed [10], [11]. Second, the control distributions are often achieved using a numerical search, which has substantial computation burden and is unsuitable for practical implementation in ground vehicles [8], [10], [11].

Most differential torque control systems are proposed for electric vehicles, which equip in-wheel motors to generate traction/braking torque for each tire independently. Thus, the designated tire forces (positive or negative) can be easily implemented by controlling the wheel torques on each tire [9], [12]. These approaches cannot be applied to two-wheel drive vehicles, in which only two front tires or two rear tires can have braking torques.

In our previous paper [13], we propose a vehicle trajectory control method using differential traction/braking torques that can be applied to four-wheel, front-steer, and front-drive vehicles. The proposed control algorithm is developed using a hierarchical architecture and can obtain four controlled wheel torques using control distribution methods, which is similar to the approaches discussed in [2], [4], and [7]–[11]. In contrast to these approaches, the proposed method achieves both robust performance and optimal control distributions. In addition, the optimal solution is obtained analytically instead of using a numerical search. However, the control inputs must chatter to meet the requirements of the robust control and optimal control distribution. In addition, the procedures used to obtain an analytical solution are not presented in [13]. This study improves the control algorithms to retain all the advantages of the previous method and to ensure that the control inputs do not chatter. In addition, this paper presents the procedures used to obtain an analytical solution from this nonlinear optimization problem, the control algorithm derivations, and the stability analysis of the proposed control system.

II. Vehicle Model for Controller Development

A vehicle model with three degrees-of-freedom (DOFs) and two coordinate systems [14], [15] is used to facilitate control algorithm derivations. These two coordinate systems are the global frame $\{\mathrm{g}\}$ and the body frame $\{\mathrm{b}\}$. Similar to conventional approaches, the global frame is fixed to a point on Earth, whereas the body frame is fixed to the center of gravity (CG) of the vehicle. This vehicle model is as in (1), shown below. The first two equations describe the vehicle translational motions in the x-axis and y-axis in the body frame. The third equation describes the vehicle yaw motions, which is used to indicate the heading direction of the vehicle. The last equation describes the relations between tire forces and the applied traction/braking torques. The definitions of each state variable and geometric parameter are listed in Table I. For clarity, a schematic plot of a vehicle and two coordinate systems are shown in Fig. 1. Thus

$$\begin{aligned} m(\ddot{x}_\mathrm{b} - \dot{\psi}\dot{y}_\mathrm{b}) &= F_{\mathrm{x}1} + F_{\mathrm{x}2} + F_{\mathrm{x}3} + F_{\mathrm{x}4} \\ m(\ddot{y}_\mathrm{b} + \dot{\psi}\dot{x}_\mathrm{b}) &= F_{\mathrm{y}1} + F_{\mathrm{y}2} + F_{\mathrm{y}3} + F_{\mathrm{y}4} \\ I_\mathrm{z}\ddot{\psi} &= l_\mathrm{f}(F_{\mathrm{y}1} + F_{\mathrm{y}2}) - l_\mathrm{r}(F_{\mathrm{y}3} + F_{\mathrm{y}4}) \\ &\quad - t_\mathrm{f}(F_{\mathrm{x}1} - F_{\mathrm{x}2}) + t_\mathrm{r}(F_{\mathrm{x}3} - F_{\mathrm{x}4}) \\ I_\omega\dot{\omega}_i &= -F_{\mathrm{a}i}r_i + T_i, \quad \text{for} \quad i = 1 \sim 4 \end{aligned} \tag{1}$$

TABLE I
Nomenclature

Symbol	Definition
x_g, $\dot{x}_\mathrm{g}$, $\ddot{x}_\mathrm{g}$	the longitudinal position/velocity/acceleration of the vehicle CG observed in the global frame
y_g, $\dot{y}_\mathrm{g}$, $\ddot{y}_\mathrm{g}$	the lateral position/velocity/acceleration of the vehicle CG observed in the global frame
$\dot{x}_\mathrm{b}$, $\ddot{x}_\mathrm{b}$	the longitudinal velocity/acceleration of the vehicle CG observed in the body frame
$\dot{y}_\mathrm{b}$, $\ddot{y}_\mathrm{b}$	the lateral velocity/acceleration of the vehicle CG observed in the body frame
ψ, $\dot{\psi}$, $\ddot{\psi}$	vehicle yaw angle/angular rate/angular acceleration
$F_{\mathrm{a}i}$, $F_{\mathrm{b}i}$	longitudinal/lateral tire force, and the subscript i refers to the four corners whereas: 1→front-left, 2 to 4 in a clockwise motion
$F_{\mathrm{x}i}$, $F_{\mathrm{y}i}$	longitudinal/lateral tire force with respect to the body frame
$F_{\mathrm{z}i}$	vertical loads of the tire i
ω_i, $\dot{\omega}_i$	angular velocity/acceleration of the tire i
T_i	wheel torque of the tire i
δ_i	wheel angle of the tire i
α_i	slip angle of the tire i
C_{yi}	cornering stiffness of the tire i
m	vehicle mass
r_i	effective radius of the tire i
I_x, I_y, I_z	the moments of inertia of the sprung mass system along the longitudinal/lateral/vertical axis
I_ω	the moments of inertia of four tires
l_f, l_r	the distances from the CG to the front/rear axes
t_f, t_r	one-half of the distances of the front/rear track

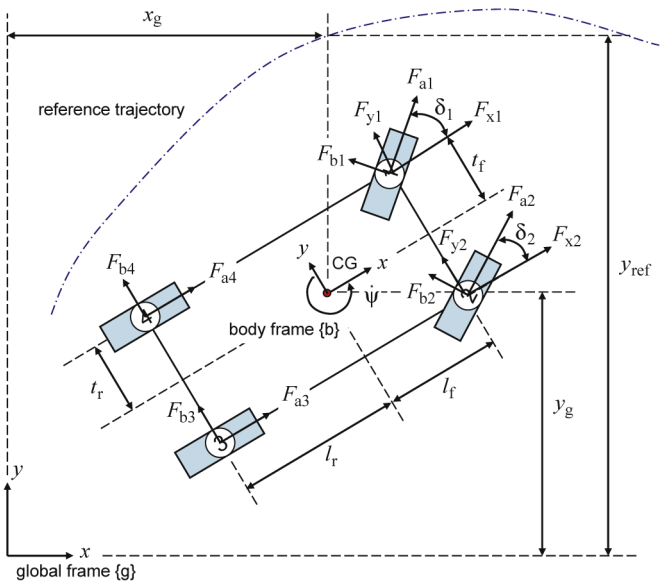

Fig. 1. Schematic plot of a vehicle and two coordinate systems (global frame and body frame). The blue dash-dotted line represents a reference trajectory.

where

$$\begin{aligned} F_{\mathrm{x}i} &= F_{\mathrm{a}i}\cos\delta_i - F_{\mathrm{b}i}\sin\delta_i \\ F_{\mathrm{y}i} &= F_{\mathrm{a}i}\sin\delta_i + F_{\mathrm{b}i}\cos\delta_i. \end{aligned}$$

For a front-steer and front-drive vehicle, the two front-wheel angles (δ_1, δ_2) are determined using the Ackerman steering principle [16], whereas the two rear-wheel angles (δ_3, δ_4) are zeros.

The longitudinal tire forces $F_{\mathrm{a}i}$ are used as the intermediate control input in this hierarchical architecture, the values of which are determined from the control algorithms. The lateral

tire force $F_{\mathrm{b}i}$ is a nonlinear function of the slip angles α_i and road friction [17], [18]. Under the assumptions of small slip angles and constant friction coefficients, the magnitude of the lateral tire force can be described using a linear tire model [18]. Thus

$$F_{\mathrm{b}i} = C_{yi}\alpha_i \tag{2}$$

where

$$\begin{aligned}
\alpha_1 &= \delta_1 - \tan^{-1}\left[(\dot{y}_{\mathrm{b}} + l_{\mathrm{f}}\dot{\psi})/(\dot{x}_{\mathrm{b}} - t_{\mathrm{f}}\dot{\psi})\right] \\
\alpha_2 &= \delta_2 - \tan^{-1}\left[(\dot{y}_{\mathrm{b}} + l_{\mathrm{f}}\dot{\psi})/(\dot{x}_{\mathrm{b}} + t_{\mathrm{f}}\dot{\psi})\right] \\
\alpha_3 &= -\tan^{-1}\left[(\dot{y}_{\mathrm{b}} - l_{\mathrm{r}}\dot{\psi})/(\dot{x}_{\mathrm{b}} + t_{\mathrm{r}}\dot{\psi})\right] \\
\alpha_4 &= -\tan^{-1}\left[(\dot{y}_{\mathrm{b}} - l_{\mathrm{r}}\dot{\psi})/(\dot{x}_{\mathrm{b}} - t_{\mathrm{r}}\dot{\psi})\right].
\end{aligned}$$

Velocities $\dot{x}_{\mathrm{b}}$, $\dot{y}_{\mathrm{b}}$ represent the velocity observed in the body frame, and velocities $\dot{x}_{\mathrm{g}}$, $\dot{y}_{\mathrm{g}}$ represent the velocity observed in the global frame. When neglecting the vehicle roll and pitch motions, the relations between the global frame and the body frame can be described by vehicle yaw angle ψ. Thus, the relations between these four velocities can be described as [19]

$$\begin{aligned}
\dot{x}_{\mathrm{g}} &= \dot{x}_{\mathrm{b}}\cos\psi - \dot{y}_{\mathrm{b}}\sin\psi \\
\dot{y}_{\mathrm{g}} &= \dot{x}_{\mathrm{b}}\sin\psi + \dot{y}_{\mathrm{b}}\cos\psi.
\end{aligned} \tag{3}$$

III. Trajectory Following Control System

Generally, two methods are used to generate a reference trajectory. The first method is "path planning," in which the reference trajectory is often obtained off-line and represented in a closed-form equation [5], [20], [21]. The second method uses an "ideal vehicle model" to generate a reference trajectory [4], [22], in which the reference trajectory can be obtained in real time. For simplicity, this study assumes that a reference trajectory is known in advance and specified in an equation. The ideal lateral position y_{ref} can be calculated by entering the current longitudinal position x_{g} into this equation. Therefore, reference trajectory following can be achieved by a lateral position control.

This study uses the differential tire forces with the DYC method for lateral position control. This DYC method is implemented using the sliding-mode control in a hierarchical architecture. The rationale for this approach is that the hierarchical architecture can simplify the controller derivation task. However, as mentioned earlier, the hierarchical architecture may introduce model errors to the control system. Thus, the sliding-mode control is used to minimize this error and other errors resulting from unmodeled system dynamics, which are explained in detail in the following sections. A control distribution method is used with the DYC method to determine the applied wheel torques on each tire. This is achieved by formulating a nonlinear optimization problem for the previously mentioned sliding-mode controls. Specifically, this controller design is developed using the following steps.

A. 3-DOF Vehicle Model With Uncertainties

The 3-DOF vehicle model shown in (1) is mainly used for control algorithm derivation. To develop a robust controller based on this simplified vehicle model, the unmodeled vehicle dynamics and uncertain vehicle parameters are added to the simplified vehicle model [1]. Therefore, the dynamics of the vehicle yaw motions shown in (1) are modified as follows:

$$\begin{aligned}
\ddot{\psi} &= A_0 + \Delta A + (\mathbf{B}_0 + \Delta\mathbf{B})(\mathbf{F}_{\mathrm{a}0} + \Delta\mathbf{F}_{\mathrm{a}}) \\
A_0 &= (F_{\mathrm{b}1}l_{\mathrm{f}}\cos\delta_1 + F_{\mathrm{b}1}t_{\mathrm{f}}\sin\delta_1 + F_{\mathrm{b}2}l_{\mathrm{f}}\cos\delta_2 \\
&\quad - F_{\mathrm{b}2}t_{\mathrm{f}}\sin\delta_2 - F_{\mathrm{b}3}l_{\mathrm{r}} - F_{\mathrm{b}4}l_{\mathrm{r}})/I_{\mathrm{z}} \\
\mathbf{B}_0 &= [B_1, \quad B_2, \quad B_3, \quad B_4] \\
&= [(l_{\mathrm{f}}\sin\delta_1 - t_{\mathrm{f}}\cos\delta_1)/I_{\mathrm{z}}, \quad (l_{\mathrm{f}}\sin\delta_2 + t_{\mathrm{f}}\cos\delta_2)/I_{\mathrm{z}} \\
&\quad t_{\mathrm{r}}/I_{\mathrm{z}}, \quad -t_{\mathrm{r}}/I_{\mathrm{z}}] \\
\Delta\mathbf{B} &= [\Delta B_1, \quad \Delta B_2, \quad \Delta B_3, \quad \Delta B_4] \\
\mathbf{F}_{\mathrm{a}0} &= [F_{\mathrm{a}1}, \quad F_{\mathrm{a}2}, \quad F_{\mathrm{a}3}, \quad F_{\mathrm{a}4}]^{\mathrm{T}}
\end{aligned} \tag{4}$$

where A_0 and $\mathbf{B}_0$ contain the original vehicle dynamics shown in (1); $\mathbf{F}_{\mathrm{a}0}$ is the designated control input; ΔA represents the uncertain value of A_0, which mainly originates from lateral tire forces; $\Delta\mathbf{B}$ represents the uncertain value of $\mathbf{B}$, which mainly originates from the neglected vehicle attitude (pitch and roll); and $\Delta\mathbf{F}_{\mathrm{a}}$ is the uncertain value of the longitudinal tire forces, which originates from two sources: 1) neglected slip ratios and varying road frictions when calculating the tire forces and 2) neglected wheel dynamics when calculating the applied wheel torques.

B. Lyapunov Function

A Lyapunov function is used to assist the subsequent control algorithm derivation to ensure system stability. To implement the DYC control strategy in this vehicle control system, Lyapunov function V is chosen to consist of the lateral displacement error and yaw rate error. Thus

$$\begin{aligned}
V &= \frac{1}{2}s^2 + \frac{1}{2}e^2 \\
s &= \dot{y}_{\mathrm{g}} - \dot{y}_{\mathrm{ref}} + \lambda(y_{\mathrm{g}} - y_{\mathrm{ref}}) \\
e &= \dot{\psi} - \dot{\psi}_{\mathrm{ref}}
\end{aligned} \tag{5}$$

where λ is a design parameter, and its value must be positive to comply with the slide mode control design rules [23]; $\dot{\psi}_{\mathrm{ref}}$ represents the reference yaw rate, and its value is determined at a later stage. To analyze system stability with this Lyapunov function, the time derivative of the Lyapunov function is calculated and regrouped into three terms, i.e.,

$$\begin{aligned}
\dot{V} &= \dot{V}_{\mathrm{p}1} + \dot{V}_{\mathrm{p}2} + \dot{V}_{\mathrm{p}3} \\
\dot{V}_{\mathrm{p}1} &= -\tau_1 s^2 - \tau_2 e^2 + \dot{x}_{\mathrm{g}} s e \\
\dot{V}_{\mathrm{p}2} &= (\ddot{x}_{\mathrm{b}}\sin\psi + \ddot{y}_{\mathrm{b}}\cos\psi)s + \dot{x}_{\mathrm{g}}\dot{\psi}_{\mathrm{ref}}s \\
&\quad - \ddot{y}_{\mathrm{ref}}s - s\lambda(\dot{y}_{\mathrm{g}} - \dot{y}_{\mathrm{ref}}) + \tau_1 s^2 \\
\dot{V}_{\mathrm{p}3} &= e\ddot{\psi} - e\ddot{\psi}_{\mathrm{ref}} + \tau_2 e^2
\end{aligned} \tag{6}$$

where τ_1, τ_2 are design parameters, and their values are chosen to make $\dot{V}_{\mathrm{p}1}$ negative semidefinite. Thus, system stability is determined by the values of $\dot{V}_{\mathrm{p}2}$ and $\dot{V}_{\mathrm{p}3}$.

C. Sliding-Mode Control Method

The reference yaw rate in (6) is designed according to the sliding-mode design procedures for system robustness, as follows:

$$\begin{aligned}\dot{\psi}_{\rm ref} &= -\dot{x}_{\rm g}^{-1}\left[-\ddot{y}_{\rm ref}-\lambda(\dot{y}_{\rm g}-\dot{y}_{\rm ref})+\tau_1 s+\kappa s/\Phi_1\right]\\ \kappa &= \sup_{t\in[0,\infty]}\left|\ddot{x}_{\rm b}(t)\sin\psi(t)+\ddot{y}_{\rm b}(t)\cos\psi(t)\right|+\eta_1 \end{aligned}\quad (7)$$

where η_1 is a design parameter, the value of which is small and positive to comply with the slide mode control design rules; Φ_1 represents an implicit boundary layer, the value of which is positive [23]. Using the reference yaw rate shown in (7), $\dot{V}_{\rm p2}$ can be rewritten as

$$\begin{aligned}\dot{V}_{\rm p2} &= (\ddot{x}_{\rm b}\sin\psi+\ddot{y}_{\rm b}\cos\psi)s-\kappa s^2/\Phi_1\\ &\le -\eta_1 s^2/\Phi_1, \qquad \text{for} \qquad |s|\ge\Phi_1. \end{aligned}\quad (8)$$

Thus, $\dot{V}_{\rm p2}$ is negative semidefinite outside the implicit boundary layer Φ_1.

Substituting (4) into (6), $\dot{V}_{\rm p3}$ can be rewritten as follows:

$$\begin{aligned}\dot{V}_{\rm p3} &= e\left[A_0+\Delta A+(\mathbf{B}_0+\Delta\mathbf{B})(\mathbf{F}_{\rm a0}+\Delta\mathbf{F}_{\rm a})-\ddot{\psi}_{\rm ref}+\tau_2 e\right]\\ &\le \overline{A}+e\mathbf{B}_0\mathbf{F}_{\rm a0}+|e|\delta_{\rm B1}|F_{\rm a1}|+|e|\delta_{\rm B2}|F_{\rm a2}|\\ &\quad +|e|\delta_{\rm B3}|F_{\rm a3}|+|e|\delta_{\rm B4}|F_{\rm a4}| \end{aligned}\quad (9)$$

where

$$\begin{aligned}\overline{A} &= eA_0+|e|\delta_{\rm A}+|e|\,\|\mathbf{B}_0\|_2\delta_{\rm F}+|e|\delta_{\rm B}\delta_{\rm F}-e\ddot{\psi}_{\rm ref}+\tau_2 e^2\\ \delta_{\rm F} &= \sup_{t\in[0,\infty]}\|\Delta\mathbf{F}_{\rm a}(t)\|_2\\ \delta_{\rm A} &= \sup_{t\in[0,\infty]}|\Delta A(t)|\\ \delta_{{\rm B}i} &= \sup_{t\in[0,\infty]}|\Delta B_i(t)|\\ \delta_{\rm B} &= \sqrt{\delta_{\rm B1}^2+\delta_{\rm B2}^2+\delta_{\rm B3}^2+\delta_{\rm B4}^2}. \end{aligned}$$

D. Control Distribution

The design of longitudinal tire forces must establish the negative semidefinite of $\dot{V}_{\rm p3}$ for system stability. The longitudinal forces on two rear tires must be nonpositive for front-drive vehicles. Several sets of longitudinal tire forces satisfy these constraints. Hence, the determination of the longitudinal force of each tire is formulated as a constrained optimization problem for an optimal solution.

1) Nonlinear Constrained Optimization: The objective of this optimization problem is to achieve minimal control efforts. Thus, it is formulated as follows:

$$\begin{aligned}\min\quad & \frac{1}{2}\mathbf{F}_{\rm a0}^{\rm T}\mathbf{Q}\mathbf{F}_{\rm a0}\\ \text{s.t.}\quad & \overline{A}+e\mathbf{B}_0\mathbf{F}_{\rm a0}+|e|\delta_{\rm B1}|F_{\rm a1}|+|e|\delta_{\rm B2}|F_{\rm a2}|\\ & +|e|\delta_{\rm B3}|F_{\rm a3}|+|e|\delta_{\rm B4}|F_{\rm a4}|=-\eta_2 e^2\\ & F_{\rm a3},F_{\rm a4}\le 0 \end{aligned}\quad (10)$$

where

$$\begin{aligned}\mathbf{Q} &= \text{diagonal}\left([q_1,q_2,q_3,q_4]\right)\\ q_i &= F_{zi}^{-1}, \qquad \text{for} \quad i=1\sim 4. \end{aligned}$$

The first constraint equation in (10) ensures the negative semidefinite of $\dot{V}_{\rm p3}$ when design parameter η_2 is set as a positive number. The second constraint equation ensures the nondriving forces on two rear tires. The first constraint only needs to be smaller than zero for system stability. However, it is intentionally formulated as an equality constraint instead of an inequality constraint. Although this more-than-necessary constraint may increase the control efforts, it reduces the size of solution pools to prevent the solution (control inputs) selected by the optimization process from jumping around, which is impractical and may damage the vehicle.

$\mathbf{Q}$ is a weighting matrix. It is designed as a diagonal matrix with elements that are equal to the inverse of the corresponding vertical loads of each tire. This approach minimizes the control efforts and justifies the small slip-ratio assumption, which is discussed further at a later stage.

2) Modifications of the Equality Constraint: Although the equality constraint prevents the control inputs from jumping around when seeking the minimal control efforts, the control inputs may still chatter in the event of unmodeled vehicle dynamics. This chattering problem is difficult to eliminate, as explained in Section V. This study proposes a novel approach to minimize the chattering problem by introducing another implicit boundary layer Φ_2 into the original constraint in (10). The modified equality constraint is written as follows:

$$\begin{aligned}&\overline{A}_2+\mathbf{B}_0\mathbf{F}_{\rm a0}+e\delta_{\rm B1}|F_{\rm a1}|/\Phi_2+e\delta_{\rm B2}|F_{\rm a2}|/\Phi_2\\ &\qquad +e\delta_{\rm B3}|F_{\rm a3}|/\Phi_2+e\delta_{\rm B4}|F_{\rm a4}|/\Phi_2+\eta_2 e=0 \end{aligned}\quad (11)$$

where

$$\overline{A}_2 = A_0+\left(\delta_{\rm A}+\|\mathbf{B}_0\|_2\delta_{\rm F}+\delta_{\rm B}\delta_{\rm F}\right)e/\Phi_2-\ddot{\psi}_{\rm ref}+\tau_2 e.$$

Therefore, the nonlinear constrained optimization problem accompanied with constraint equation (11) can achieve the negative semidefinite of $\dot{V}_{\rm p3}$ outside the boundary layer Φ_2 but achieves the negative semidefinite of $\dot{V}_{\rm p3}$ globally when accompanied with constraint (10). The numerical simulations will demonstrate the performance difference due to these two constraint equations.

E. Analytical Solution

Because of the absolute values shown in (10) and (11), the problem is a nonlinear optimization, and its solution is primarily obtained using a numerical search. A numerical search is less preferred in vehicle real-time applications. Therefore, this nonlinear optimization problem is further processed using variable transformation and the Karush–Kuhn–Tucker (KKT) theorem to obtain its analytical solution.

1) Variable Transformation: Variable transformation is used to remove the absolute values shown in (10) and (11). Thus, the nonlinear optimization problem can be converted into a quadratic optimization problem with equality and inequality constraints [24]. Thus

$$\begin{aligned}F_{an} &= F_{an}^{+}-F_{an}^{-}\\ |F_{an}| &= F_{an}^{+}+F_{an}^{-}, \qquad \text{for} \quad n=1,2 \end{aligned}\quad (12)$$

where

$$F_{an}^{+}=\begin{cases}F_{an}, & \text{if } F_{an}>0\\ 0, & \text{if } F_{an}\le 0\end{cases}$$
$$F_{an}^{-}=\begin{cases}0, & \text{if } F_{an}>0\\ -F_{an}, & \text{if } F_{an}\le 0\end{cases}$$
$$F_{an}^{+},F_{an}^{-}\ge 0.$$

When substituting (12) into (10), the constrained optimization problem can be rewritten as

$$\begin{aligned}\min\quad & \frac{1}{2}\left[q_1^2\left(F_{\mathrm{a1}}^{+}-F_{\mathrm{a1}}^{-}\right)^2+q_2^2\left(F_{\mathrm{a2}}^{+}-F_{\mathrm{a2}}^{-}\right)^2+q_3^2F_{\mathrm{a3}}^2+q_4^2F_{\mathrm{a4}}^2\right]\\ \text{s.t.}\quad & C+\mathbf{D}\overline{\mathbf{F}}_{\mathrm{a}}=0\\ & -F_{\mathrm{a1}}^{+},-F_{\mathrm{a1}}^{-},-F_{\mathrm{a2}}^{+},-F_{\mathrm{a2}}^{-},F_{\mathrm{a3}},F_{\mathrm{a4}}\le 0\end{aligned}\tag{13}$$

where

$$\begin{aligned}C&=\overline{A}+\eta_2e^2\\ \mathbf{D}&=\left[D_1^{+},D_1^{-},D_2^{+},D_2^{-},D_3,D_4\right]\\ &=[eB_1+|e|\delta_{\mathrm{B1}},-eB_1+|e|\delta_{\mathrm{B1}},eB_2+|e|\delta_{\mathrm{B2}},\\ &\quad -eB_2+|e|\delta_{\mathrm{B2}},eB_3-|e|\delta_{\mathrm{B3}},eB_4-|e|\delta_{\mathrm{B4}}]\\ \overline{\mathbf{F}}_{\mathrm{a}}&=\left[F_{\mathrm{a1}}^{+},F_{\mathrm{a1}}^{-},F_{\mathrm{a2}}^{+},F_{\mathrm{a2}}^{-},F_{\mathrm{a3}},F_{\mathrm{a4}}\right]^{\mathrm{T}}.\end{aligned}$$

For comparison, we also apply the state transformation to the modified constraint in (11). The resulting equations are also casted in the $(C+\mathbf{D}\,\overline{\mathrm{F}}_{\mathrm{a}}=0)$ format. The corresponding $(C,\ \mathbf{D})$ and optimization problem are as follows:

$$\begin{aligned}\min\quad & \frac{1}{2}\left[q_1^2\left(F_{\mathrm{a1}}^{+}-F_{\mathrm{a1}}^{-}\right)^2+q_2^2\left(F_{\mathrm{a2}}^{+}-F_{\mathrm{a2}}^{-}\right)^2+q_3^2F_{\mathrm{a3}}^2+q_4^2F_{\mathrm{a4}}^2\right]\\ \text{s.t.}\quad & C+\mathbf{D}\overline{\mathbf{F}}_{\mathrm{a}}=0\\ & -F_{\mathrm{a1}}^{+},-F_{\mathrm{a1}}^{-},-F_{\mathrm{a2}}^{+},-F_{\mathrm{a2}}^{-},F_{\mathrm{a3}},F_{\mathrm{a4}}\le 0\\ & C=\overline{A}_2+\eta_2e\\ & \mathbf{D}=[B_1+e\delta_{\mathrm{B1}}/\Phi_2,-B_1+e\delta_{\mathrm{B1}}/\Phi_2,B_2+e\delta_{\mathrm{B2}}/\Phi_2\\ & \quad -B_2+e\delta_{\mathrm{B2}}/\Phi_2,B_3-e\delta_{\mathrm{B3}}/\Phi_2,B_4-e\delta_{\mathrm{B4}}/\Phi_2].\end{aligned}\tag{14}$$

2) KKT Theorem: The KKT theorem has proven that an optimal solution or a local minimizer can be obtained for a nonlinear optimization problem subjected to the equality and inequality constraints [25]. Although the solution may not be the global minimum, system stability is guaranteed because the stability requirements are formulated as the constraint equations in this optimization problem.

Consider the following example:

$$\begin{aligned}\min\quad & \mathbf{f}(\mathbf{x})\\ \text{s.t.}\quad & \mathbf{h}(\mathbf{x})=\mathbf{0}\\ & \mathbf{g}(\mathbf{x})\le\mathbf{0}\end{aligned}$$

where $\mathbf{x}\in\Re^{\mathrm{n}}$, $\mathbf{f}:\Re^{\mathrm{n}}\to\Re$, $\mathbf{h}:\Re^{\mathrm{n}}\to\Re^{\mathrm{m}}$, $\mathrm{m}\le\mathrm{n}$, and $\mathbf{g}:\Re^{\mathrm{n}}\to\Re^{\mathrm{p}}$. According to the theorem, local minimizer $\mathbf{x}^*$ must meet the following KKT conditions [25]:

$$\begin{aligned}\boldsymbol{\mu}&\ge\mathbf{0}\\ \nabla\mathbf{f}(\mathbf{x}^*)+\boldsymbol{\lambda}_{\mathrm{L}}^{\mathrm{T}}\nabla\mathbf{h}(\mathbf{x}^*)+\boldsymbol{\mu}^{\mathrm{T}}\nabla\mathbf{g}(\mathbf{x}^*)&=\mathbf{0}^{\mathrm{T}}\\ \boldsymbol{\mu}^{\mathrm{T}}\mathbf{g}(\mathbf{x}^*)&=0\\ \mathbf{h}(\mathbf{x}^*)&=\mathbf{0}\\ \mathbf{g}(\mathbf{x}^*)&\le\mathbf{0}\end{aligned}\tag{15}$$

where $\boldsymbol{\mu}$ is the KKT multiplier vector, and $\boldsymbol{\lambda}_{\mathrm{L}}$ is the Lagrange multiplier vector. The first, third, and fifth equations in (15) ensure that the KKT multipliers μ_i are positive when the corresponding inequality constraints are active $(\mathbf{g}(\mathbf{x}^*)=\mathbf{0})$ and are zeros when the corresponding inequality constraints are inactive $(\mathbf{g}(\mathbf{x}^*)<\mathbf{0})$.

For the nonlinear optimization problem shown in (13), the KKT conditions are

$$\begin{aligned}q_1^2\left(F_{\mathrm{a1}}^{+}-F_{\mathrm{a1}}^{-}\right)+\lambda_1D_1^{+}-\mu_1&=0\\ -q_1^2\left(F_{\mathrm{a1}}^{+}-F_{\mathrm{a1}}^{-}\right)+\lambda_1D_1^{-}-\mu_2&=0\\ q_2^2\left(F_{\mathrm{a2}}^{+}-F_{\mathrm{a2}}^{-}\right)+\lambda_1D_2^{+}-\mu_3&=0\\ -q_2^2\left(F_{\mathrm{a2}}^{+}-F_{\mathrm{a2}}^{-}\right)+\lambda_1D_2^{-}-\mu_4&=0\\ q_3^2F_{\mathrm{a3}}+\lambda_1D_3+\mu_5&=0\\ q_4^2F_{\mathrm{a4}}+\lambda_1D_4+\mu_6&=0\\ -\mu_1F_{\mathrm{a1}}^{+}-\mu_2F_{\mathrm{a1}}^{-}-\mu_3F_{\mathrm{a2}}^{+}-\mu_4F_{\mathrm{a2}}^{-}+\mu_5F_{\mathrm{a3}}+\mu_6F_{\mathrm{a4}}&=0\\ C+\mathbf{D}\overline{\mathbf{F}}_{\mathrm{a}}&=0\\ -F_{\mathrm{a1}}^{+},-F_{\mathrm{a1}}^{-},-F_{\mathrm{a2}}^{+},-F_{\mathrm{a2}}^{-},F_{\mathrm{a3}},F_{\mathrm{a4}}&\le 0\end{aligned}\tag{16}$$

where λ_1 and $\mu_{1\sim6}$ are the corresponding Lagrange multiplier and KKT multipliers of (13), respectively. When searching for the optimal solution, (16) must be repeatedly solved for each case: $\mu_i=0,\mu_i\ne0,i=1\sim6$; that is, $2^6=64$ times. However, in this vehicle control problem, the number can be reduced to 2 by following three guidelines: 1) Both F_{an}^{+} and F_{an}^{-} cannot be zeros according to their definitions in (12); 2) at both the front end and back end, the tire forces on the left and right tires cannot have the same sign for vehicle yaw motions; and 3) at both the right and left sides of the vehicle, the front and rear tire forces cannot have different signs for minimal power consumption. Consequently, only two possible combinations remain, and the corresponding solutions are

$$\begin{aligned}&\text{Case I}\quad(\mu_1=0,\mu_2\ne0,\mu_3\ne0,\mu_4=0,\mu_5=0,\mu_6\ne0)\\ &F_{\mathrm{a1}}^{+}=-\lambda_1D_1^{+}/q_1^2 && \mu_2=\lambda_1\left(D_1^{+}+D_1^{-}\right)\\ &F_{\mathrm{a1}}^{-}=0 && \mu_3=\lambda_1(D_2^{+}+D_2^{-})\\ &F_{\mathrm{a2}}^{+}=0 && \mu_6=-\lambda_1D_4\\ &F_{\mathrm{a2}}^{-}=-\lambda_1D_2^{-}/q_2^2\\ &F_{\mathrm{a3}}=-\lambda_1D_3/q_3^2\\ &F_{\mathrm{a4}}=0\\ &\lambda_1=C/\left(D_1^{+2}/q_1^2+D_2^{-2}/q_2^2+D_3^2/q_3^2\right).\\ &\text{Case II}\quad(\mu_1\ne0,\mu_2=0,\mu_3=0,\mu_4\ne0,\mu_5\ne0,\mu_6=0)\\ &F_{\mathrm{a1}}^{+}=0 && \mu_1=\lambda_1\left(D_1^{+}+D_1^{-}\right)\\ &F_{\mathrm{a1}}^{-}=-\lambda_1D_1^{-}/q_1^2 && \mu_4=\lambda_1\left(D_2^{+}+D_2^{-}\right)\\ &F_{\mathrm{a2}}^{+}=-\lambda_1D_2^{+}/q_2^2 && \mu_5=-\lambda_1D_3\\ &F_{\mathrm{a2}}^{-}=0\\ &F_{\mathrm{a3}}=0\\ &F_{\mathrm{a4}}=-\lambda_1D_4/q_4^2\\ &\lambda_1=C/\left(D_1^{-2}/q_1^2+D_2^{+2}/q_2^2+D_4^2/q_4^2\right).\end{aligned}\tag{17}$$

In Case I, the combination of the tire forces produces a negative yaw moment on the vehicle, which drives the vehicle into a left-hand turn. In Case II, it produces a positive yaw moment on the vehicle and drives the vehicle into a right-hand turn.

F. Wheel Torque Calculation

According to the wheel dynamics shown in (1), determining the exact applied wheel torques from the designated longitudinal tire forces is unrealistic because it is a noncausal process. However, by assuming small slip ratios ($\dot{\omega}_i \approx 0$), the applied wheel torque can be approximated by the following:

$$T_i = F_{\mathrm{a}i} r_i. \tag{18}$$

This approximation results in a discrepancy between the designated tire forces and the tire forces generated by the applied wheel torques. This discrepancy is managed using two approaches: 1) The longitudinal tire force is chosen to be proportional to the vertical loads in the control distribution process, which justifies the assumption of small slip ratio to some extent; and 2) the discrepancy is considered in $\Delta \mathbf{F}_{\mathrm{a}}$ in (4), and its effect is compensated by the proposed controller design.

From the derivation, the three components of $\dot{V}$ in (6) are guaranteed to be negative semidefinite when sliding surface (s) goes outside the implicit boundary layer Φ_1 and yaw rate error (e) goes outside the implicit boundary layer Φ_2. Therefore, the stability of this control system is guaranteed.

IV. Simulation Result

A. Reference Trajectory and Real Vehicle Dynamics

A "double-lane change" is used as a reference trajectory to demonstrate the feasibility of this control algorithm. In this example, a vehicle moves at an initial speed of 25 m/s ($\equiv$ 90 km/h) and has no steering angle ($\delta_1 = \delta_2 = 0$). The control algorithm is activated at the initial time to regulate the vehicle motion from one lane to another and back to the original lane. The distance between these two parallel lanes is 3 m. This reference trajectory is shown in Fig. 3(a) and can be described by the following equation [5]:

$$y_{\mathrm{ref}}(x) = \frac{3}{1+\exp^{-0.08(x-145)}} - \frac{3}{1+\exp^{-0.08(x-385)}}.$$

Two vehicle models are used to mimic real vehicle dynamics on the road: the full-state vehicle model and the E-class sedan model from Carsim 7.1 commercial software. The full-state vehicle model is a nonlinear 6-DOF vehicle model and consists of 20 states [26]. It differs from the 3-DOF vehicle model in the roll, pitch, vertical motions, and tire model. This well-documented full-state vehicle model can provide detailed information on the vehicle dynamics. Therefore, it is used to verify the concept of the control algorithm in detail. By contrast, the Carsim model is not fully open to end users; however, it is closer to real vehicle dynamics. Therefore, it is used to demonstrate the feasibility of the proposed control algorithms when applied to real vehicles. The geometric parameters of these two vehicle models are the same, as shown in Table II.

The proposed control algorithms are developed from a simplified 3-DOF vehicle model and tested on both the full-state vehicle model and Carsim model. To verify the robustness of the proposed control algorithm, we examine the performance difference among three vehicle models. In Fig. 2, the top plot shows the maneuvering of the steering wheel angle when the vehicle is moving at a speed of 25 m/s ($\equiv$ 90 km/h). The second to fourth plots show the corresponding longitudinal velocity, lateral velocity, and vehicle yaw rate of three vehicle models. The plots show that the vehicle dynamics of these three models considerably differ. Thus, the developed control algorithms must have robustness if it can be successfully applied to vehicles with different dynamics.

TABLE II
Geometric Parameters

Geometry Parameters	Simulated Vehicle Model	Geometry Parameters	Simulated Vehicle Model
m	2013 kg	l_{f}	1.402 m
I_{x}	614 $kg \cdot m^2$	l_{r}	1.646 m
I_{y}	2765 $kg \cdot m^2$	t_{f}	0.8 m
I_{z}	2765 $kg \cdot m^2$	t_{r}	0.801 m
I_{ω}	0.9 $kg \cdot m^2$	C_{y1}, C_{y2}[a]	106209 N/rad
r_i	0.364 m	C_{y3}, C_{y4}	95868 N/rad

[a] From the nonlinear tire model used in both simulated vehicle models, the cornering stiffness of the tires is calculated with respect to the static vertical loads of the corresponding tires.

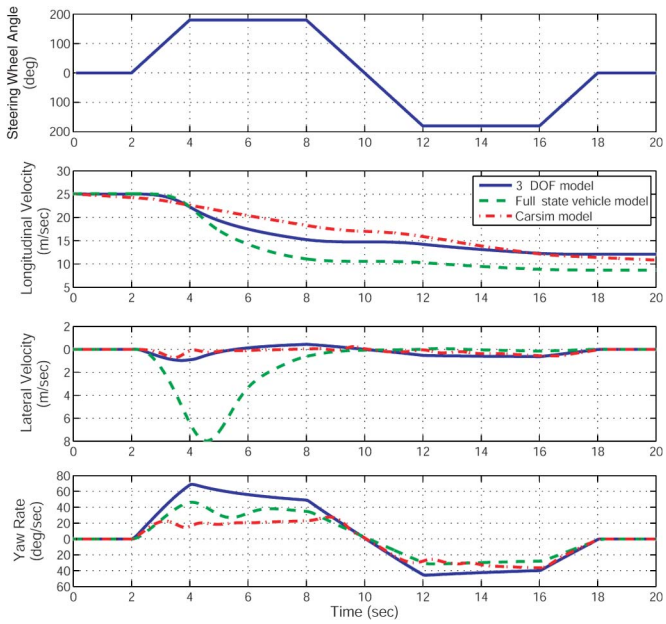

Fig. 2. Performance difference among 3-DOF vehicle model, full-state vehicle model, and E-class sedan model from Carsim. The first plot shows the maneuvering of the steering wheel angle; the second to fourth plots show the corresponding longitudinal velocity, lateral velocity, and yaw rate of three vehicle models.

The longitudinal tire forces saturate at approximately 4 kN in both full-state vehicle model and Carsim model. To focus on the feasibility study of the proposed control algorithm, the conditions of the following simulations are arranged such that the requested longitudinal tire forces are smaller than their saturation values. The sampling frequency of the vehicle control system is 100 Hz. The design parameters of the controller, which ensure the robust performance of the vehicle control system, are shown in Table III. The values are obtained from the simulation results using the full-state vehicle model. In Figs. 3, 7, and 11, the reference trajectory and reference yaw rate are shown as blue dashed lines, and the vehicle dynamics regulated by the proposed control algorithm are shown as red solid lines.

TABLE III
DESIGN PARAMETERS

Design Parameters	Value	Design Parameters	Value
λ	0.5	κ	10
η_1	0.1	η_2	0.1
Φ_1	1	Φ_2	0.01
τ_1	7.5	τ_2	22
δ_{A}	0.8	$\delta_{\mathrm{B1}\sim4}$	8e-6
δ_{F}	800		

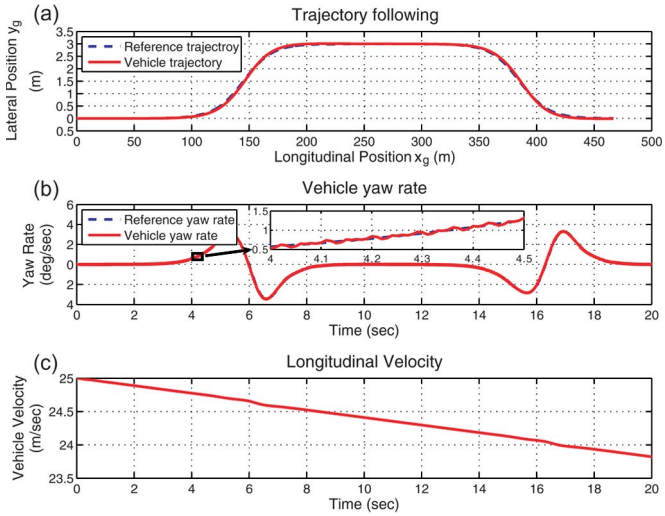

Fig. 3. (a) Trajectory following in a "double-lane change" when applying the proposed control algorithms to a full-state vehicle model. (b) The regulated vehicle yaw rate closely follows its reference yaw rate. (c) The longitudinal velocity decreases from 25 to 23.8 m/s.

B. Simulations With the Full-State Vehicle Model

Fig. 3 shows the simulation results when applying the proposed control algorithms and optimization statement (13) to a full-state vehicle model. The simulation results show that the control system successfully leads the vehicle to complete a "double-lane change," whereas the vehicle yaw rate closely follows its reference yaw rate, and the longitudinal velocity decreases from 25 to 23.8 m/s. The standard deviation of the lateral position error is 3.2 cm.

Fig. 4 shows the controlled wheel torques on each tire. As shown in the figure, the two front tires have driving and braking torques, whereas the two rear tires only have braking torques. Furthermore, the controlled torques exhibit high-frequency chattering. To remove control input chattering, a conventional and intuitive approach is to add a low-pass filter after the calculated wheel torques. The spectrum of the calculated wheel torques is first calculated to determine the desired passband of this filter design, as shown in Fig. 5. Because the chattering occurs at frequencies of approximately 25 Hz and other useful content is below 5 Hz, the bandwidth of the low-pass filter is set to 5 Hz. A discrete-time first-order low-pass filter with a passband of 5 Hz and a sampling frequency of 100 Hz is shown as follows:

$$G_{\mathrm{LPF}}(z) = \frac{0.2696z^{-1}}{1 - 0.7304z^{-1}}. \tag{19}$$

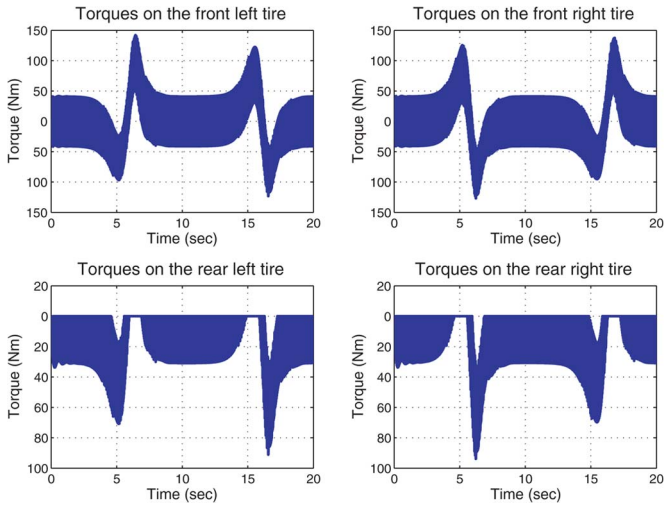

Fig. 4. Four controlled wheel torques calculated using the proposed control algorithm. The four wheel torques differ, and the torques on the two rear wheels are less than zero for front-drive vehicles.

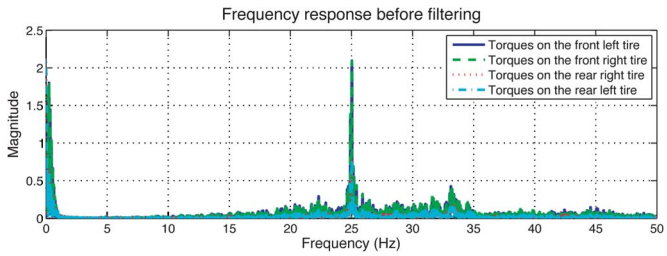

Fig. 5. Spectrum of the four controlled wheel torques. The controlled wheel toques chatter at frequencies of approximately 25 Hz.

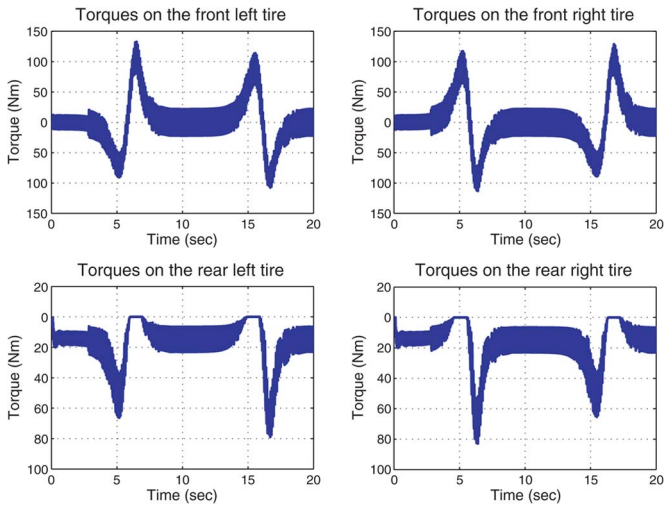

Fig. 6. Four controlled wheel torques calculated using the proposed control algorithm and a 5-Hz low-pass filter. The calculated wheel torques chatter at frequencies of approximately 12.5 Hz.

Fig. 6 shows the controlled wheel torques from the proposed controller and the filter design. As shown in the figure, the control inputs still chatter with reduced amplitude and frequencies of approximately 12.5 Hz. This is because the filter design lowers the bandwidth of the feedback path. The calculated control inputs chatter at another frequency to compensate system uncertainties. The conventional low-pass filter approach cannot

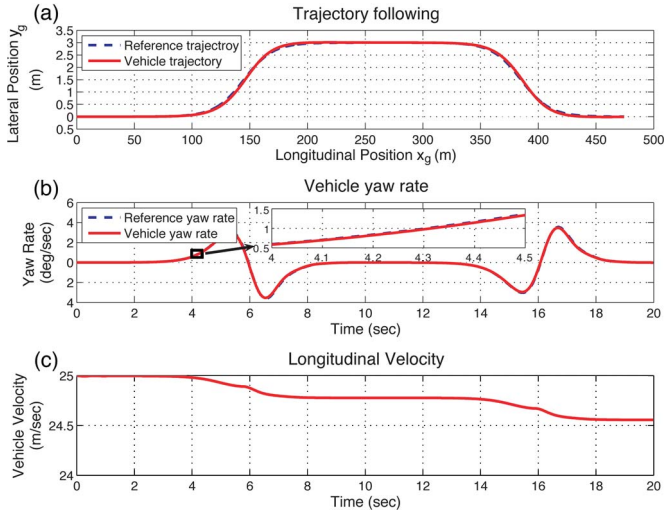

Fig. 7. (a) Trajectory following in a "double-lane change" when applying the proposed control algorithms with the modified constraint optimization to a full-state vehicle model. (b) The regulated vehicle yaw rate closely follows its reference yaw rate. (c) The longitudinal velocity decreases from 25 to 24.6 m/s.

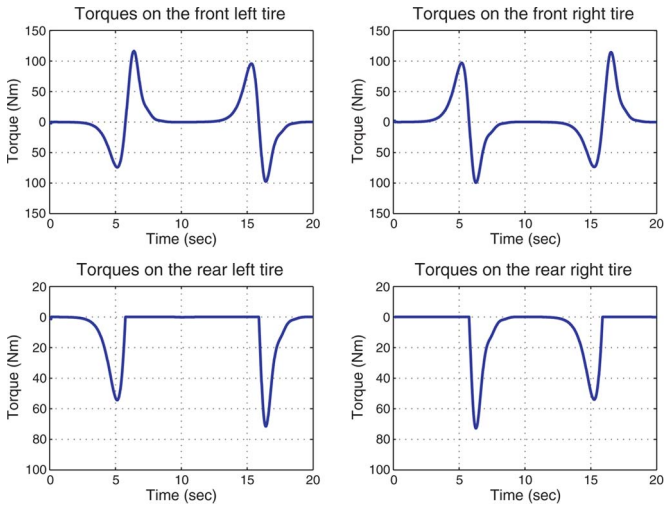

Fig. 8. Four controlled wheel torques calculated using the proposed control algorithm and the modified constraint optimization. The high-frequency chattering disappears.

be applied to this case. Another possible solution is to use a high-order low-pass filter with a smaller bandwidth. However, it may considerably induce time delay to the feedback loop and cause a stability problem.

The proposed method uses modified constraint optimization (14) instead of (13). As shown in Fig. 7, the control system successfully leads the vehicle to complete a "double-lane change," whereas the vehicle yaw rate closely follows its reference yaw rate, and the longitudinal velocity decreases from 25 to 24.6 m/s. The controlled wheel torques (see Fig. 8) do not have high-frequency chattering. The standard deviation of the lateral position error is 3.2 cm in the simulations.

In another simulation where the vehicle makes a quicker "double-lane change," as shown in Fig. 9, the control system successfully leads the vehicle to complete a "double-lane change," and the longitudinal velocity decreases from 25 to 22.0 m/s. The maximum lateral acceleration of the vehicle is

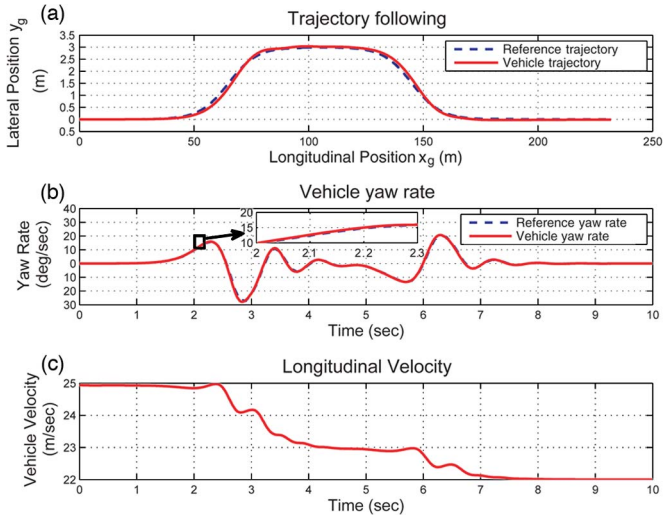

Fig. 9. (a) Trajectory following in a severe "double-lane change." The maximum lateral acceleration is 6.56 m/s^2. (b) The regulated vehicle yaw rate closely follows its reference yaw rate when applying the proposed control algorithm with the modified constraint optimization. (c) The longitudinal velocity decreases from 25 to 22.0 m/s.

6.56 m/s^2 during maneuvering. The standard deviation of the lateral position error is 6.9 cm in the simulations.

C. Simulations With the Carsim Model

Fig. 10 shows a schematic of applying the proposed controller to an E-class sedan using the Simulink/MATLAB simulation tool. Because modified constrained optimization (14) exhibits superior performance to (13), we only include the results using constrained optimization (14) in this paper.

Fig. 11 shows that the proposed control system successfully leads the vehicle to complete a "double-lane change." The vehicle yaw rate closely follows its reference yaw rate, and the longitudinal velocity decreases from 25 to 15.3 m/s. The considerable decrease in longitudinal velocity only occurs in this case because large feedback gains ($\tau_1 = 1.56$, $\tau_2 = 100$) are used to compensate for the dynamics difference between the 3-DOF vehicle model and the vehicle model from Carsim. The standard deviation of the lateral position error is 1.9 cm. Fig. 12 shows the controlled wheel torques on each tire. The controlled wheel torques do not have high-frequency chattering.

V. Discussion

The optimization process (13) induces high-frequency chattering on the wheel torques, which can be understood as follows. The constraint equation $(C + \mathbf{D}\,\overline{\mathbf{F}}_{\mathrm{a}} = 0)$ in (13) can be divided by error e to obtain the following:

$$M + (\eta_2 + \tau_2)e + \mathbf{N}\overline{\mathbf{F}}_{\mathrm{a}} = 0 \tag{20}$$

where

$$\begin{aligned} M &= A_0 + (\delta_{\mathrm{A}} + \|\mathbf{B}_0\|_2\delta_{\mathrm{F}} + \delta_{\mathrm{B}}\delta_{\mathrm{F}})\,\mathrm{sign}(e) - \ddot{\psi}_{\mathrm{ref}} \\ \mathbf{N} &= [B_1 + \delta_{\mathrm{B1}}\mathrm{sign}(e), -B_1 + \delta_{\mathrm{B1}}\mathrm{sign}(e) \\ &\quad B_2 + \delta_{\mathrm{B2}}\mathrm{sign}(e), -B_2 + \delta_{\mathrm{B2}}\mathrm{sign}(e) \\ &\quad B_3 - \delta_{\mathrm{B3}}\mathrm{sign}(e), B_4 - \delta_{\mathrm{B4}}\mathrm{sign}(e)]\,. \end{aligned}$$

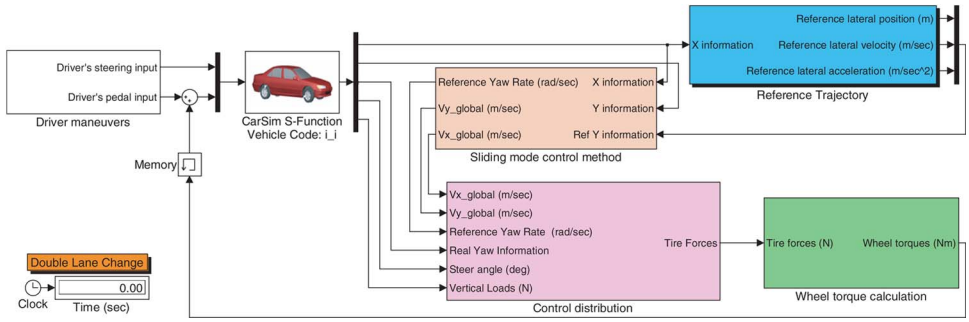

Fig. 10. Block diagram showing the application of the proposed controller to a Carsim model using the Simulink/MATLAB simulation tool.

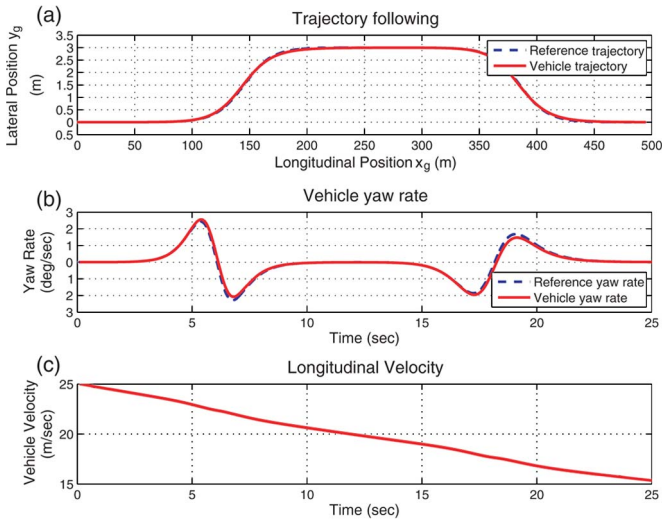

Fig. 11. (a) Trajectory following in a "double-lane change" when applying the proposed control algorithms with the modified constraint optimization to a Carsim vehicle model. (b) The regulated vehicle yaw rate closely follows its reference yaw rate. (c) The longitudinal velocity decreases from 25 to 15.3 m/s.

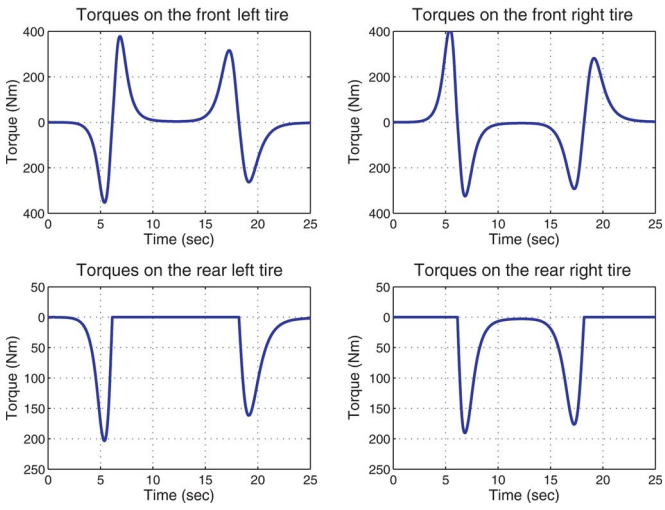

Fig. 12. Four controlled wheel torques calculated using the proposed control algorithm for application to a Carsim vehicle model.

Because this constraint must be satisfied during the optimization process, the determination of tire forces $\overline{\mathbf{F}}_{\mathrm{a}}$ is dominated by both M and $\mathbf{N}$ when e is small. The components in $\mathbf{N}$ are almost constants because of the small design parameters $\delta_{B1\sim4}$. When the vehicle does not substantially change its moving directions, both A_0 and $\ddot{\psi}_{\mathrm{ref}}$ are close to zeros. In this case, the magnitude of M is determined by the uncertainty bounds (δ_{A}, δ_{B}, and δ_{F}), and the sign of M is determined by the sign of e. Consequently, the control inputs $\overline{\mathbf{F}}_{\mathrm{a}}$ considerably chatter when the value of e is small and change signs frequently.

As suggested by the previous discussion, a method to reduce this chattering is to use smaller values of uncertainty bounds (δ_{A}, δ_{B}, and δ_{F}) or smaller values of $B_{1\sim4}$. Smaller values of uncertainty bounds imply precise modeling of the vehicle dynamics, which increases the complexity of the controller design. On the other hand, smaller values of $B_{1\sim4}$ change the vehicle configuration and cause difficulty in vehicle maneuvering, which are impractical. The proposed method solves this problem by introducing an implicit boundary layer Φ_2 into constraint equation (14). Consequently, the control input chatter occurs when error e is jumping around at either Φ_2 or $-\Phi_2$, if it does. However, with larger e, design parameters η_2 and τ_2 also participate in determining the control inputs, which reduces the chattering in the control inputs regardless of whether error e quickly oscillates.

The simulation results shown in Fig. 8 indicate that the applied wheel torques on the right tires are larger than those on the left tires when the vehicle makes a left-hand turn at 5.1 and 16.3 s; the applied torques on the left tires are larger than those on the right tires when the vehicle makes a right-hand turn at 6.2 and 15.2 s. Furthermore, the front torques are larger than the rear torques. These torque distributions occur because the CG of the vehicle is close to the front of the vehicle, and we intentionally distribute the controlled tire force with respect to the vertical loads on each tire. Fig. 13 shows the relationship among slip ratio, longitudinal force, and vertical loads from a tire model in Carsim. As shown in the figure, the longitudinal tire forces are proportional to the vertical loads on the tire when the slip ratio is fixed; the slip ratio is inversely proportional to the vertical loads when delivering a fixed longitudinal force. Therefore, distributing tire forces with respect to the vertical loads minimizes the control efforts and ensures a small slip ratio in most driving conditions. A small slip ratio implies a small variation of the tire angular rate. This justifies the approximation made in (18).

Generally, two concerns are addressed in implementing a controller design for real-time applications: availability of the system state information and the computation time. As shown in Section III, several vehicle dynamics are required to implement the proposed controller design, including longitudinal

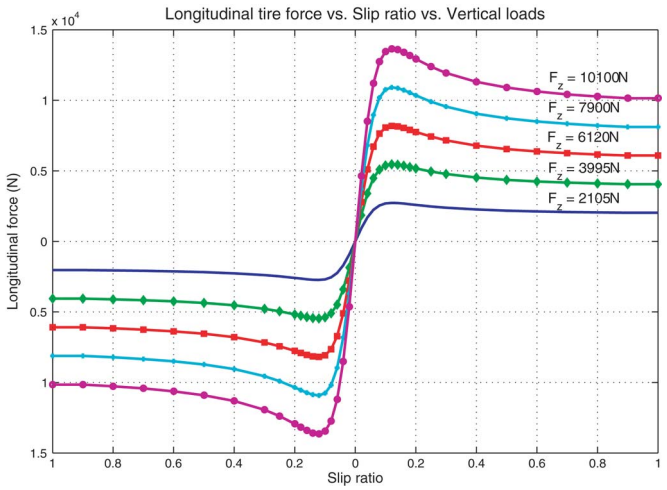

Fig. 13. Relationship among slip ratio, longitudinal tire force, and vertical loads from a tire model in Carsim.

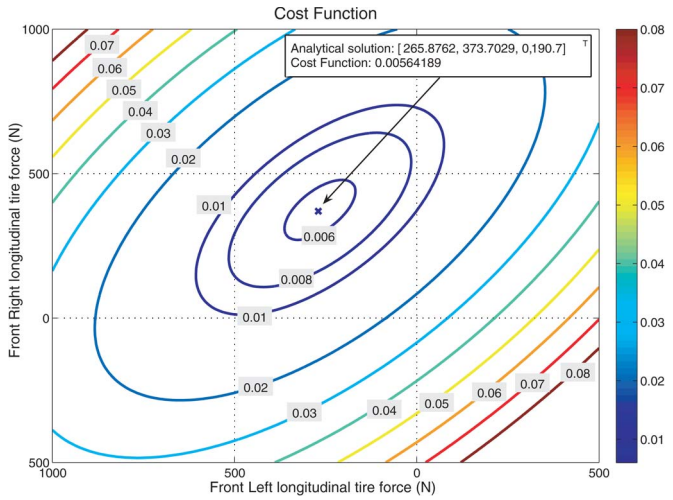

Fig. 14. Cost function contour plot for the optimal solution search.

position and velocity in the global frame (x_{g} and $\dot{x}_{\mathrm{g}}$), lateral position and velocity in the global frame (y_{g} and $\dot{y}_{\mathrm{g}}$), vertical loads on each tire ($F_{\mathrm{z}i}$), and vehicle yaw angle and angular rate (ψ and $\dot{\psi}$). The measurement accuracy of those vehicle dynamics may affect the performance of the controller design to some extent. Several studies show that vehicle dynamics with acceptable accuracy can be obtained using sensor fusion systems or state estimation systems [5], [26], [28], [29]. Because the measurement system of the vehicle dynamics is beyond the scope of this paper, we assume that these vehicle dynamics with satisfactory measurement accuracy are available for the controller design. The proposed control algorithms are shown in (5), (7), (13), (14), and (17). According to these equations, the calculations of control inputs can be completed within 150 add/multiplication steps. An entry level of the digital signal processor can complete a multiplication operation within 20 ns. Therefore, the computation time for each sampling interval is less than 10 μs, which is feasible for the 10-ms sampling time of this feedback controller design.

To verify the optimality of solution (17), we conduct a numerical search instead of convex/concave analysis of the vehicle system because the system is highly nonlinear. This optimization problem involves four parameters ($F_{\mathrm{a}1\sim4}$) and one equality constraint ($C + \mathbf{D}\,\overline{\mathbf{F}}_{\mathrm{a}} = 0$). The search space is large, and the search results are unsuitable for graphical presentation. Therefore, $F_{\mathrm{a}3}$ is assumed to be zero [case II in (17)], and $F_{\mathrm{a}4}$ is calculated using the equality constraint. Thus, the problem becomes a 2-D numerical search problem. $F_{\mathrm{a}1}$ and $F_{\mathrm{a}2}$ are used as two independent parameters changing from -1000 N to 500 N and from -500 N to 1000 N, respectively. The search results are presented by a contour plot of cost function corresponding to each data point. According to the plot shown in Fig. 14, the minimal cost function among search points is 0.006, whereas the corresponding cost function of the analytical solution is 0.00564. Therefore, if the search range is sufficiently large and the searched data points are sufficiently dense, (17) can be considered the optimal solution to this problem.

The proposed wheel torque distribution is "optimal" only under our problem definition. Further work on control algorithm derivations or vehicle modeling may even minimize the applied wheel torques in regulating the vehicle trajectory. For example, the proposed method considers the lateral tire force as uncertainty for the simplicity of determining the applied wheel torques. By contrast, detailed modeling of the lateral tire force in deriving the control algorithm may achieve smaller applied wheel torques at the expense of requiring additional information on the slide slip angle, an approximate tire model, and complicated control algorithms. The complicated control algorithms are justified for severe vehicle maneuvering. We are in the process of investigating details.

VI. Conclusion

A trajectory following control system for front-drive front-steer vehicles is developed and verified using simulations. The proposed method uses differential traction/braking torques to regulate a vehicle along a reference trajectory and minimize the control efforts. The control inputs are obtained from analytical solutions instead of from numerical search. In the proposed method, the minimal power consumption of differential torque actuation is achieved by using the DYC control strategy, control distribution with respect to the vertical loads, and nonlinear optimizations. The stability and robustness of the control system are ensured by formulating a sliding-mode control into a nonlinear optimization process. Finally, the analytical solution is obtained by using the KKT theorem to solve the nonlinear optimization problem.

Because of the nature of the optimization and sliding-mode controls, the proposed method is prone to large control input chattering. This occurs because the optimization process requires control inputs to quickly switch to minimize control efforts, and the sliding-mode control also requests control inputs to quickly switch to compensate for the effect caused by system uncertainties. The conventional approach of adding a low-pass filter cannot solve this problem. The proposed method solves this problem by using an equality constraint equation with an implicit boundary layer in the sliding-mode controls instead of the frequently used inequality constraint equation and sign functions.

The proposed control algorithms are tested both on a full-state vehicle model and an E-class sedan model from Carsim. In both cases, the vehicle moves at an initial speed of 90 km/h. The proposed method can regulate the vehicle to complete a "double-lane change" with the maximum lateral acceleration of 6.56 m/s^2 and the lateral position error less than 6.9 cm.

REFERENCES

[1] H. Du, N. Zhang, and G. Dong, "Stabilizing vehicle lateral dynamics with considerations of parameter uncertainties and control saturation through robust yaw control," *IEEE Trans. Veh. Technol.*, vol. 59, no. 5, pp. 2593–2597, Jun. 2010.

[2] W. Cho, J. Choi, C. Kim, S. Choi, and K. Yi, "Unified chassis control for the improvement of agility, maneuverability, and lateral stability," *IEEE Trans. Veh. Technol.*, vol. 61, no. 3, pp. 1008–1020, Mar. 2012.

[3] C. Zhao, W. Xiang, and P. Richardson, "Vehicle lateral control and yaw stability control through differential braking," in *Proc. IEEE ISIE*, Montréal, QC, Canada, 2006, pp. 384–389.

[4] V. Cerone, M. Milanese, and D. Regruto, "Yaw stability control design through a mixed-sensitivity approach," *IEEE Trans. Control Syst. Technol.*, vol. 17, no. 5, pp. 1096–1104, Sep. 2009.

[5] M. Schorn, U. Stählin, A. Khanafer, and R. Isermann, "Nonlinear trajectory following control for automatic steering of a collision avoiding vehicle," in *Proc. Amer. Control Conf.*, Minneapolis, MN, USA, 2006, pp. 5837–5842.

[6] Y. Hayakawa, R. White, T. Kimura, and G. Naito, "Driver-compatible steering system for wide speed-range path following," *IEEE/ASME Trans. Mechatronics*, vol. 9, no. 3, pp. 544–552, Sep. 2004.

[7] D. Piyabongkarn, J. Y. Lew, R. Rajamani, J. A. Grogg, and Q. Yuan, "On the use of torque-biasing systems for electronic stability control: Limitations and possibilities," *IEEE Trans. Control Syst. Technol.*, vol. 15, no. 3, pp. 581–589, May 2007.

[8] J. Tjnnås and T. A. Johansen, "Stabilization of automotive vehicles using active steering and adaptive brake control allocation," *IEEE Trans. Control Syst. Technol.*, vol. 18, no. 3, pp. 545–558, May 2010.

[9] J. Kang, J. Yoo, and K. Yi, "Driving control algorithm for maneuverability, lateral stability, and rollover prevention of 4WD electric vehicles with independently driven front and rear wheels," *IEEE Trans. Veh. Technol.*, vol. 60, no. 7, pp. 2987–3011, Sep. 2011.

[10] E. Ono, Y. Hattori, Y. Muragishi, and K. Koibuchi, "Vehicle dynamics integrated control for four-wheel-distributed steering and four-wheel-distributed traction/braking systems," *Veh. Syst. Dyn.*, vol. 44, no. 2, pp. 139–151, 2006.

[11] J. Andreasson and T. Bünte, "Global chassis control based on inverse vehicle dynamics models," *Veh. Syst. Dyn.*, vol. 44, no. Suppl. 1, pp. 321–328, 2006.

[12] Y. Chen and J. Wang, "Design and evaluation on electric differentials for overactuated electric ground vehicles with four independent in-wheel motors," *IEEE Trans. Veh. Technol.*, vol. 61, no. 4, pp. 1534–1542, May 2012.

[13] L.-Y. Hsu and T.-L. Chen, "A constrained wheel torque controller for lane following system using control distribution," in *Proc. Amer. Control Conf.*, 2010, pp. 997–1002.

[14] B. A. Guvenc, L. Guvenc, and S. Karaman, "Robust yaw stability controller design and hardware-in-the-loop testing for a road vehicle," *IEEE Trans. Veh. Technol.*, vol. 58, no. 2, pp. 555–571, Feb. 2009.

[15] T. Chung and K. Yi, "Design and evaluation of side slip angle-based vehicle stability control scheme on a virtual test track," *IEEE Trans. Control Syst. Technol.*, vol. 14, no. 2, pp. 224–234, Mar. 2006.

[16] W. Norris, *Modern Steam Road Wagons*. London, U.K.: Longmans, 1906, pp. 63–67.

[17] A. Porcel, P. Laurence, M. Basset, and G. L. Gissinger, "Tyre model for vehicle simulation: Overview and real time solution for critical situations," in *Proc. IEEE Conf. Control Appl.*, 2001, pp. 817–822.

[18] H. Dugoff, P. S. Fancher, and L. Segel, "An analysis of tire traction properties and their influence on vehicle dynamic performance," presented at the Soc. Automotive Eng. Int. Conf., Detroit, MI, USA, Feb. 1970, SAE Paper 700 377.

[19] K. T. Feng, "Vehicle lateral control for driver assistance and automated driving," Ph.D. dissertation, Dept. Mech. Eng., Univ. Calfornia, Berkeley, CA, USA, 2000.

[20] P. Setlur, J.-R. Wagner, D.-M. Dawson, and D. Braganza, "A trajectory tracking steer-by-wire control system for ground vehicles," *IEEE Trans. Veh. Technol.*, vol. 55, no. 1, pp. 76–85, Jan. 2006.

[21] S.-A. Arogeti and N. Berman, "Path following of autonomous vehicles in the presence of sliding effects," *IEEE Trans. Veh. Technol.*, vol. 61, no. 4, pp. 1481–1492, May 2012.

[22] D. Kim, S. Hwang, and H. Kim, "Vehicle stability enhancement of four-wheel-drive hybrid electric vehicle using rear motor control," *IEEE Trans. Veh. Technol.*, vol. 57, no. 2, pp. 727–735, Mar. 2008.

[23] J. E. Slotine and W. Li, *Applied Nonlinear Control*. Englewood Cliffs, NJ, USA: Prentice-Hall, 1991.

[24] R. L. Rardin, *Optimization in Operations Research*. Englewood Cliffs, NJ, USA: Prentice-Hall, 1998.

[25] E. K. P. Chong and S. H. Żak, *An Introduction to Optimization*. New York, NY, USA: Wiley-Interscience, 2001.

[26] L.-Y. Hsu and T.-L. Chen, "Vehicle full-state estimation and prediction system using state observers," *IEEE Trans. Veh. Technol.*, vol. 58, no. 6, pp. 2651–2662, Jul. 2009.

[27] L.-Y. Hsu and T.-L. Chen, "Applying a three-antenna GPS and suspension displacement sensors to a road vehicle," in *Proc. IEEE Conf. Sens.*, 2009, pp. 1593–1597.

[28] S. Alban, "An inexpensive and robust GPS/INS system for automobiles," in *Proc. ION-GPS*, Portland, OR, USA, 2002, pp. 1075–1087.

[29] J. Ryu and J. C. Gerdes, "Integrating inertial sensors with GPS for vehicle dynamics control," *ASME J. Dyn. Syst., Meas., Control*, vol. 126, no. 2, pp. 243–254, Jun. 2004.

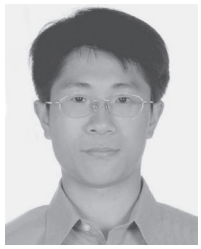

Ling-Yuan Hsu received the B.S. and M.S. degrees in mechanical engineering from National Chiao Tung University, Hsinchu, Taiwan, in 2004 and 2006, respectively, where he is currently working toward the Ph.D. degree.

Since 2006, he has been with the Department of Mechanical Engineering, National Chiao Tung University.

Tsung-Lin Chen received the B.S. and M.S. degrees in power mechanical engineering from National Tsing Hua University, Hsinchu, Taiwan, in 1990 and 1992, respectively, and the Ph.D. degree in mechanical engineering from the University of California, Berkeley, Berkeley, CA, USA, in 2001.

From 2001 to 2002, he was a MEMS Design Engineer with Analog Devices Inc. Since 2003, he has been with the Department of Mechanical Engineering, National Chiao Tung University, Hsinchu, where he is currently an Associate Professor. His research interests include microelectromechanical systems and controls.